The role of the capping agent and nanocrystal size in photoinduced hydrogen evolution using CdTe/CdS quantum dot sensitizers

View Article Online
DOI: 10.1039/D0DT01195A

ARTICLE

On the role of the capping agent and nanocrystal size in photoinduced hydrogen evolution using CdTe/CdS quantum dots sensitizers

Received 00th January 20xx,
Accepted 00th January 20xx

DOI: 10.1039/x0xx00000x

Elisabetta Benazzi,*[a] Valerio C. Coni, [a] Mattia Boni, [a] Raffaello Mazzaro,[b] Vittorio Morandi,[b] and Mirco Natali *[a,c]

Hydrogen production via light-driven water splitting is a key process in the context of solar energy conversion. In this respect the choice of suitable light-harvesting units appears as a major challenge, particularly as far as stability issues are concerned. In this work we report on the use of CdTe/CdS QDs as photosensitizers for light-assisted hydrogen evolution in combination with a nickel bis(diphosphine) catalyst (**1**) and ascorbate as the sacrificial electron donor. QDs of different sizes (between 1.7-3.4 nm) and with different capping agents (**MPA**, **MAA**, and **MSA**) have been prepared and their performance assessed in the above-mentioned photocatalytic reaction. Detailed photophysical studies have been also accomplished to highlight the charge transfer processes relevant to the photocatalytic reaction. Hydrogen evolution is observed with remarkable efficiencies when compared to common coordination compounds like $Ru(bpy)_3^{2+}$ (where bpy = 2,2'-bipyridine) as light-harvesting units. Furthermore, the hydrogen evolution performance under irradiation is strongly determined by the nature of the capping agent and the QD size and can be related to the concentration of surface defects within the semiconducting nanocrystal. Overall, the present results outline how QDs featuring large quantum yields and long lifetimes are desirable to achieve sustained hydrogen evolution upon irradiation and that a precise control of the structural and photophysical properties thus appears as a major requirement towards profitable photocatalytic applications.

Introduction

The economic progress and the constant demographic increase in the world population have led to a drastic enhancement in the global energy demand. How to meet this request has become a central topic for scientific research. The use of fossil fuels would imply a further increase in atmospheric carbon dioxide levels with catastrophic consequences on climate change.[1] The solution to the energy problem must be an energy source which is abundant, cheap, and with low environmental impact. Solar energy is the most suitable candidate for this purpose: it has an irradiating power of 120,000 TW and in nature is used to support photosynthetic organisms capable of converting carbon dioxide and water into carbohydrates and molecular oxygen (natural photosynthesis).[2] Hence, the development of an efficient artificial photosynthetic system, generating fuel with sunlight, can provide a valid alternative to tackle the global energy issue.

The use of hydrogen as an energy vector, in particular, is a technically feasible approach.[3,4] A direct method for generating hydrogen and oxygen via water splitting using solar irradiation is under development. However, important challenges still need to be addressed before a low-cost, highly efficient, and environmentally benign technology is established. To achieve the reductive side of water splitting, a number of approaches have been investigated. Most extensively studied are molecular and/or materials-based systems.[5-10] Concerning molecular ones, light-driven proton reduction to dihydrogen can be driven by systems consisting of three main components: a sacrificial electron donor (SED), a light harvesting unit (PS), and a hydrogen evolution catalyst (HEC).[11-13] These systems provide a unique way to test new sensitizer and/or catalyst units and allow for a favourable description of mechanistic aspects related to the coupling of such components in view of potential applications.[11] The appropriate choice of the photosensitizer is a crucial parameter in light-driven proton reduction. Complexes of ruthenium(II), iridium(III), rhenium(I), or platinum(II)[14-22] and metalloporphyrins[23-30] are among the most widely employed chromophores. However, one of the vital problems of these systems is the low stability along H_2 generation in aqueous solutions, due to competitive decomposition pathways. From this viewpoint, quantum dots may represent a valid alternative. Quantum dots (QDs), also known as semiconductor nanocrystals, are under heavy investigation in many research fields due to their unique optical properties such as broad absorption and narrow emission with peak positions tuneable by their sizes and bandwidth controllable to a certain degree by their size distribution.[31] QDs preparation requires the

[a] Department of Chemical and Pharmaceutical Sciences, University of Ferrara, Via L. Borsari 46, 44121, Ferrara, Italy. E-mail: elisabetta.benazzi@unife.it, mirco.natali@unife.it.
[b] CNR-IMM Bologna, Via P. Gobetti 101, 40139 Bologna, Italy.
[c] Centro Interuniversitario per la Conversione Chimica dell'Energia Solare (SolarChem), sez. Di Ferrara, Via L. Borsari 46, 44121 Ferrara, Italy.
Electronic Supplementary Information (ESI) available: cyclic voltammetry, results from TC-SPC, other photocatalytic results. See DOI: 10.1039/x0xx00000x

View Article Online
DOI: 10.1039/D0DT01195A

nucleation in the nm scale of the semiconducting material through the use of suitable stabilizing agents that cover the surface of the QDs acting as protective layer. Furthermore, by varying the chemical nature of the surface agent it is possible to select the environment in which the QDs can be solubilized. Photocatalytic hybrid systems that combine molecular catalysts and semiconductor nanoparticles, such as CdX (where X = S, Se, Te),[32-37] ZnS,[38,39] and CdSe/ZnS[40] as well as cadmium-free $CuInS_2$/ZnS[41] as light-harvesting materials, have been successfully reported in recent years. From this perspective, the use of CdTe QDs as sensitizers for hydrogen evolution is not common and limited to a few cases. In the first reports, MPA-capped CdTe QDs have been used in combination with natural hydrogenases for the production of hydrogen under visible-light irradiation.[42,43] A system based on CdTe QDs has been studied by Sun and co-workers, coupled to cobalt catalysts characterized by sulfur-based binders to promote the formation of sensitizer/catalyst hybrids.[44] This approach was extremely favourable, showing high activity towards the reduction of protons to hydrogen with remarkable stability. At the same time, Llobet and co-workers studied in detail the photocatalytic performance and mechanism of hydrogen evolution promoted by CdTe QDs in combination with a macrocyclic cobalt complex as a HEC.[45] However, a thorough understanding of the impact of the particle size, stabilizing agents, etc. of QDs on the photocatalytic performance of related three-component systems is currently elusive. Starting from these considerations, in this work we have studied light-driven hydrogen evolution in a three-component system composed of mixed CdTe/CdS QDs as sensitizers, a nickel Dubois complex (**1**) as catalyst (HEC),[46,47] and ascorbate as the sacrificial electron donor (Scheme 1).

Scheme 1. Summary of the components used in this study and related working principles.

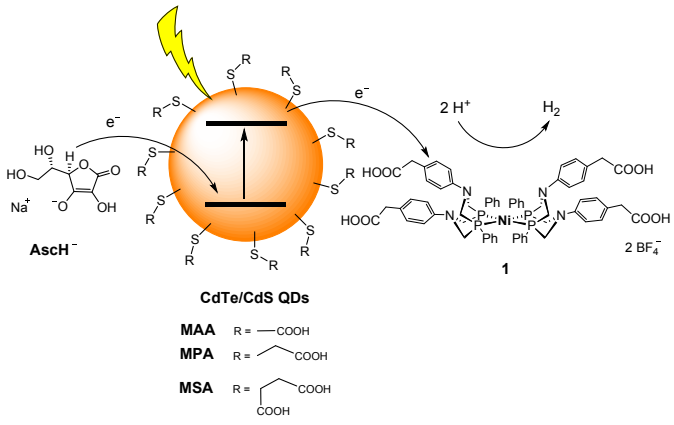

QDs of different sizes have been prepared using three different stabilizing agents. The assessment of the photocatalytic properties towards hydrogen evolution along with the corresponding photophysical characteristics suggests that minimization of the surface defects of the semiconducting nanocrystal is imperative in order to attain enhanced hydrogen evolution under illumination.

Results and discussion

Synthesis and characterization.

The synthesis of the QDs has been carried out in aqueous solution using an established protocol, by reaction of $CdCl_2$ and K_2TeO_3 in the presence of a capping agent and $NaBH_4$.[48] Three different stabilizing agents have been used (Scheme 1): mercaptopropionic acid (**MPA**), mercaptosuccinic acid (**MSA**), and mercaptoacetic acid (**MAA**). Since the properties of the resulting QDs are expected to depend on the molar ratio of the reactants, pH, temperature, etc., we have adopted the optimized conditions used by Wu and co-workers[48] (see Experimental Section). By controlling the reaction time, QDs having specific optical properties have been obtained. In all three cases, as the reaction time increases, a red shift of both the absorption and the emission occurs which is attributed to the narrowing of the band gap as a result of the increase in the nanoparticle size. In Figure 1a are displayed the absorption spectra of QDs with **MPA** capping agent obtained at different reaction time, while in Figure 1b are reported the corresponding emission profiles. These spectral profiles are consistent with the obtainment of water-soluble QDs.[48]

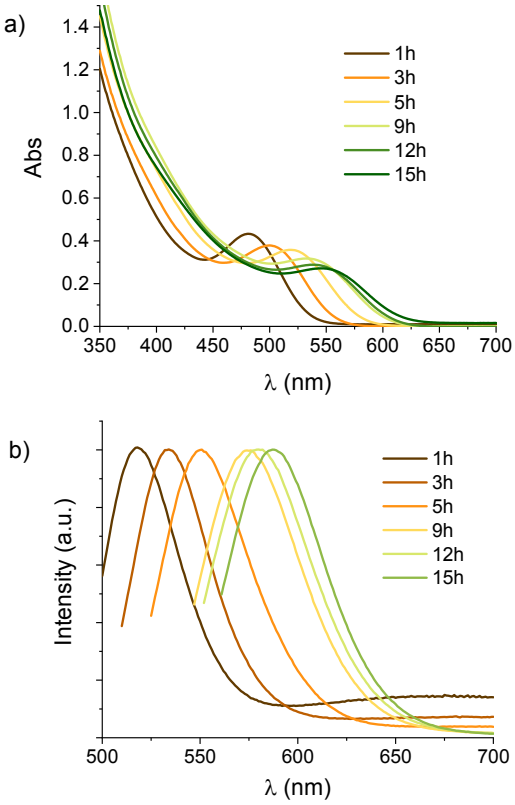

Fig. 1. a) Absorption and b) emission spectra of **MPA** QDs (2.6-8.9 μM depending on the size)[50] in aqueous solution at pH 10.5 (excitation was performed at the excitonic absorption maximum).

The absorption spectra for all samples are characterized by a featuring band in the visible region (with maxima between 450-600 nm depending on the sample), attributable to the excitonic transition, and an absorption tail at shorter wavelengths. The emission spectra show a main contribution arising from the

View Article Online
DOI: 10.1039/C5DT01195A

direct exciton deactivation, characteristic of QDs based on cadmium chalcogenides and characterized by a small Stokes shift, plus some less intense contributions at longer wavelengths, particularly evident for short reaction times, attributable to emission from trap states.[49] Similar trends have been observed for both the **MAA**- and **MSA**-capped QDs (Figure S1 and S2, respectively), although the reaction proceeds faster using **MSA** as a stabilizing agent. To evaluate the photocatalytic properties of QDs towards hydrogen evolution, we have decided to isolate samples with two specific sizes for all the three capping agents with absorption maxima in the range 510-520 and 550-570 nm and corresponding to nanocrystals featuring either green or yellow luminescence, respectively. For these samples, using an established protocol,[50] it is possible to estimate an average diameter of the nanoparticles of 2.7(±0.1) and 3.3(±0.1) nm, respectively. At the same time different **MPA**-capped QDs featuring absorption maxima at 481 nm, 502 nm, and 538 nm have been also isolated for the photocatalytic tests, corresponding to nanoparticles with average diameters of 1.7, 2.4, and 3.1 nm.[50] For all these samples, emission quantum yields have been estimated using either rhodamine or fluorescein as standards (Table 1).[51] Furthermore, time-resolved emission decays have been recorded by TC-SPC (Figure S3-S11). As expected, the decays are not mono-exponential and have been fitted using a tri-exponential function. An average lifetime (<τ>) has been estimated as the weighted average of the three components (Table 1). From these data it is possible to calculate the values of both the radiative (k_R) and non-radiative rate constants (k_{NR}).

Table 1. Emission quantum yield (Φ), lifetime (τ), radiative (k_R) and non-radiative rate constants (k_{NR}) of **MAA**, **MPA** and **MSA** QDs.

QDs [a]	τ (ns) [b]	Φ [c]	k_R (10^7 s^{-1}) [d]	k_{NR} (10^7 s^{-1}) [e]
MAA, d = 2.6 nm	14	0.13	0.9	6.2
MAA, d = 3.2 nm	17	0.20	1.2	4.4
MSA, d = 2.8 nm	24	0.35	1.4	2.7
MSA, d= 3.4 nm	36	0.32	0.9	1.9
MPA, d = 1.7 nm	15	0.14	0.9	6.5
MPA, d = 2.4 nm	19	0.23	1.2	4.1
MPA, d = 2.8 nm	27	0.30	1.1	2.6
MPA, d = 3.1 nm	35	0.38	1.1	1.7
MPA, d = 3.3 nm	44	0.49	1.1	1.2

[a] Diameters have been calculated according to ref. 50 from the absorption spectrum; [b] weighted average lifetime from a triexponential fitting; [c] calculated using either rhodamine 6G (ethanol) or fluorescein (0.1 M NaOH) as standards; [d] calculated from the equation $\Phi = k_R \cdot \tau$; [e] calculated from the equation $\tau = 1/(k_R+k_{NR})$.

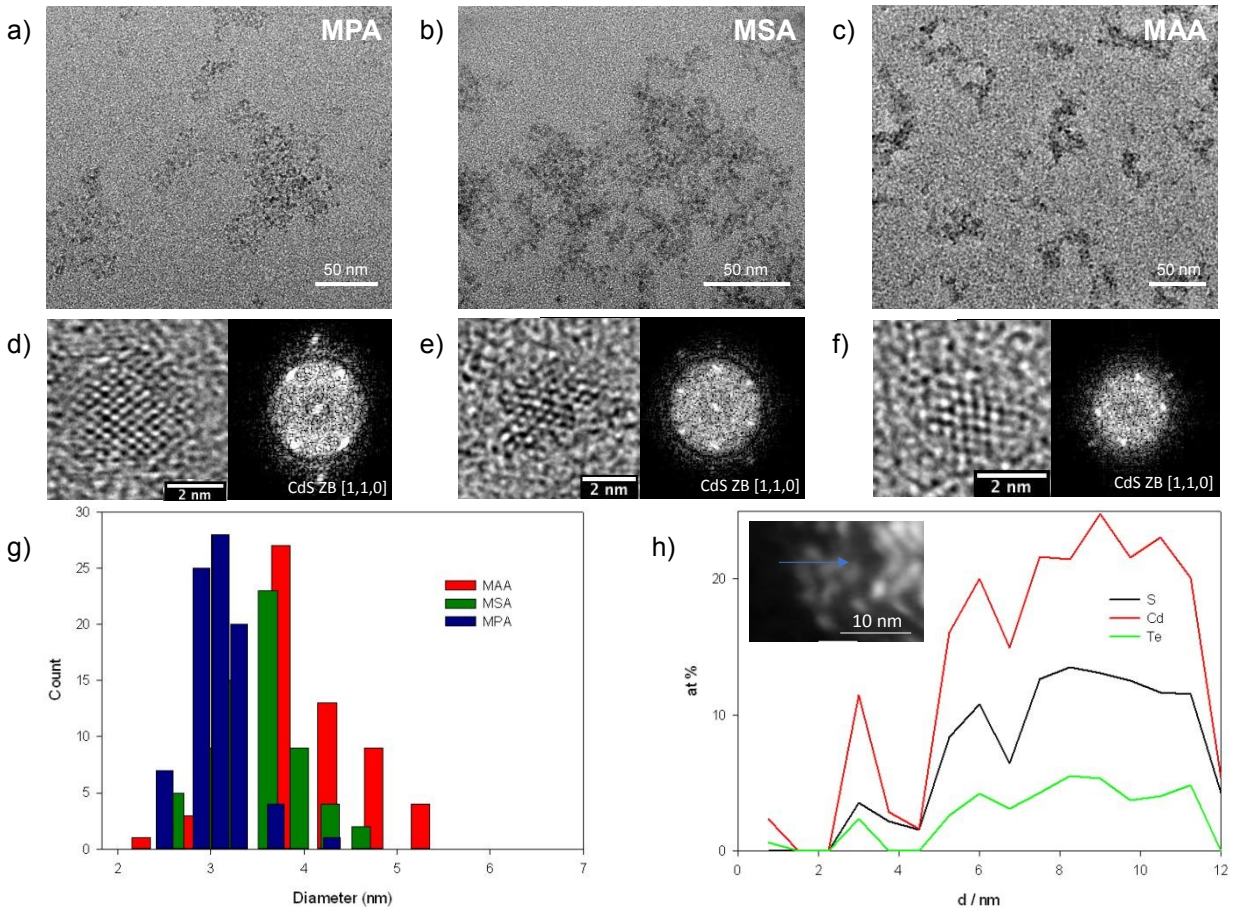

Fig. 2. Low magnification TEM images of a) **MPA**-, b) **MSA**-, and c) **MAA**-capped QDs; d,e,f) high magnification HR-TEM detail of a single quantum dot and relative Fast Fourier Transform for **MPA**-, **MSA**-, and **MAA**-capped QDs, respectively, displaying in all cases the typical pattern of [1,1,0] CdS Zincblende cubic phase; g) size distribution analysis obtained in STEM-HAADF mode of **MPA**-, **MSA**-, and **MAA**-capped QDs; h) elemental distribution along a linear profile of **MAA**-capped QDs, displayed in the reference STEM-HAADF micrograph in the inset, in which Cd, S, and Te distribution is reported to understand QDs composition.

View Article Online
DOI: 10.1039/D0DT01185A

A closer inspection of the emission data clearly suggests that the radiative constants are appreciably independent of the capping agent and nanoparticle size (~10^7 s^{-1}). On the contrary, the non-radiative rate constant increases from **MPA**- to **MSA**- and finally to **MAA**-capped QDs, while it decreases with increasing nanoparticle size for all samples. This trend is in apparent contradiction with energy-gap-law considerations and can be explained in terms of different content of surface defects.[52] A high concentration of surface defects involves the presence of intra band-gap electronic states which act as favourable intermediates towards exciton deactivation and electron-hole recombination.

Combined HR-TEM and EDS analyses have been performed on all the differently capped QDs featuring the most red-shifted absorption in order to obtain additional information on the QDs morphology and composition. Low magnification TEM images on the three QD samples are depicted in Figure 2a,b and c and show only slight aggregation due to the deposition process. EDS analysis (Table S1) confirms the presence of Cd, Te, and S within all samples. The relative concentration is also reported, but it should be considered qualitative due to the limited size of the nanocrystal. An increasing Te content is evidenced by shifting from **MPA**-capped QDs to **MSA**- and **MAA**-capped ones. The elements are homogeneously distributed along the QDs, as displayed by the STEM-EDS profile reported in figure 2h. Cd, S and Te-related signals are indeed simultaneously rising upon performing the EDS analysis on a single QD (**MAA**-capped sample reported as example). Size distribution analysis was then performed based on STEM micrographs (Figure 2g). Average diameters of 3.0(±0.4), 3.8(±0.9), and 3.5(±0.7) nm can be estimated for **MPA**-, **MAA**-, and **MSA**-capped QDs, in fairly good agreement with the theoretically predicted values.[50] HR-TEM micrographs have been collected to obtained further insight into the QD composition. Interestingly, all QDs are crystalline in nature, as displayed by the relative Fast Fourier transform (Figure 2d,e,f), which displays the typical diffraction fringes of single domain nanocrystals. However, the pattern observed are mainly compatible with the crystal lattice of CdS phases, in particular with Zincblende (cubic) for all QDs and Wurtzite (hexagonal) for **MAA**-capped QDs only. This is consistent with the XRD analysis reported by Wu and co-workers[48] on the same QDs and can be similarly attributed to the formation of a thick CdS shell onto a CdTe core occurring via degradation of the sulfur-based capping agent during the course of the reaction. The possibility of CdS to act as a protective shell for the CdTe core might effectively passivate the CdTe QD surface and explain the progressive enhancement in terms of luminescence quantum yield and lifetime observed upon increasing the QDs size (see above, Table 1).[48] Nevertheless, we also ought to consider that the present results, and in particular the observed homogeneous elemental distribution (Figure 2h), strongly support the hypothesis that, instead of core-shell nanoparticles, the synthetic procedure here adopted leads to the formation of nanoparticles featuring a mixed CdS/CdTe phase in which Te^{2-} anions act as dopant of CdS QDs.[53,54] However, since the decomposition of the capping agent occurs in parallel with the growth of the CdTe nanocrystal, it is very likely that contribution from a CdS phase might be particularly relevant for QDs of larger size such as the ones examined herein. Thus, in this latter option, a higher CdS content with increasing the QD size may be beneficial towards the improvement in the luminescence properties, as experimentally observed.

Thermodynamic considerations

Before investigating the performance of the three-component system with respect to light-driven hydrogen evolution, we first evaluated the thermodynamic feasibility of the whole photochemical process. This can be conceived as a series of consecutive one-electron redox reactions in which the electrons supplied by the ascorbate donor are used for the reduction of two protons to dihydrogen through the use of light and a catalyst. A general energy scheme relevant to the photocatalytic reduction of hydrogen promoted by QDs as sensitizers in combination with the Dubois-type catalyst **1** and ascorbate ($AscH^-$) as a sacrificial agent is shown in Scheme 2.

Scheme 2. Photocatalytic mechanism for H_2 production using QDs as sensitizers, ascorbic acid as the sacrificial agent and **1** as the catalyst: a) first and b) second electron transfer sequence.

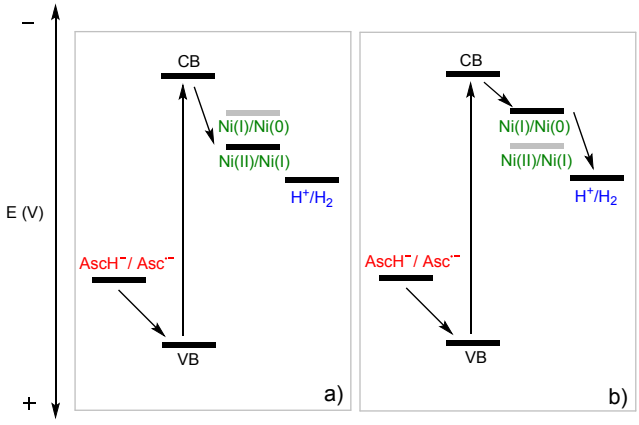

The excitation of QDs involves an electron promotion from the valence band (VB) to the conduction band (CB), the hole in the VB has to be filled by electron transfer from the ascorbate donor, the electron in the CB has to be employed for the reduction of the catalyst. This process has to take place twice to allow the accumulation of two reducing equivalents on the catalyst which is thus able to carry out the two-electron reduction of protons to hydrogen.

The redox processes involving protons and ascorbate are of proton-coupled electron transfer (PCET) nature, therefore they are pH dependent (E (H^+/H_2) = 0 V and E($Asc^{\bullet-}/AscH^-$) = +0.71 V vs NHE at pH 0).[55,56] Concerning the nickel complex **1**, the relevant potentials to be considered, measured in acetonitrile, are E (Ni(II)/Ni(I)) = −0.25 V vs NHE and E(Ni(I)/Ni(0)) = −0.41 V vs NHE, according to the most likely EECC catalytic mechanism.[46] In order to determine the potentials associated to the CB and VB of all QDs considered, we employed a procedure recently reported by Llobet and co-workers.[45] The potential values estimated are reported in Table 2. We have first

View Article Online
DOI: 10.1039/D0DT01105A

estimated the spectroscopic energy (E^{00}) from the intersection between the normalized absorption and the emission spectra (Figure 1, S1, and S2). Then, cyclic voltammetry of the samples under anodic scan (Figure S12-S14) has been performed to extract the VB potential. This value is comparable among the series of QDs and also to the one for **MPA**-capped CdTe QDs previously reported (+0.94 V vs. NHE, as obtained by CV).[45] Then, the difference between the potential of the VB and the spectroscopic energy yields the potential of the CB (Table 2).¶ From the data collected, it can be argued that all the photoinduced electron transfer processes leading to hydrogen formation are thermodynamically allowed for all samples. In particular, the ET from the ascorbate donor to the VB displays comparable driving forces independently of the size and capping agent used. On the contrary, the ET from the CB to the catalyst **1** becomes more exergonic upon reduction of the nanocrystal size. The capping agent has a marginal, but non-negligible role in the energetics of the ET from the QDs CB to the catalyst, with **MAA** QDs samples displaying slightly larger driving forces than **MPA** and lastly than **MSA**.

Table 2. Valence band potential (E_{VB}), conduction band potential (E_{CB}), and spectroscopic energy (E^{00}) of QDs.

QDs	E_{VB} (V) [a]	E_{CB} (V) [b]	E^{00} (eV)
MAA, d = 2.6 nm	+1.00	−1.30	2.30
MAA, d = 3.2 nm	+1.02	−1.17	2.19
MSA, d = 2.8 nm	+1.00	−1.23	2.23
MSA, d = 3.4 nm	+1.01	−1.10	2.10
MPA, d = 1.7 nm	+0.99	−1.31	2.30
MPA, d = 2.4 nm	+1.01	−1.24	2.25
MPA, d = 2.8 nm	+1.00	−1.21	2.21
MPA, d = 3.1 nm	+0.99	−1.20	2.19
MPA, d = 3.3 nm	+1.01	−1.13	2.14

[a] Potentials estimated by CV (see Figure S12, S13, and S14) and referenced to NHE upon addition of +0.24 V; [b] estimated as the difference between the oxidation potential and the spectroscopic energy E^{00}.

Light-driven hydrogen evolution

The photocatalytic performances have been assessed upon visible-light irradiation of aqueous solutions of QDs with a suitable size and with the proper capping agent as directly obtained from the synthetic protocol reported above. Addition of catalyst **1** and the appropriate amounts of ascorbic acid and sodium ascorbate buffer to provide a pH = 5 has been made prior to oxygen removal (by purging with Ar) and subsequent irradiation. The choice of the pH conditions is dictated by a two-fold reason: i) pH 5 is the optimum pH for hydrogen evolution in aqueous solution catalysed by the nickel complex **1**,[46] ii) at lower pH **MAA**, **MPA**, and **MSA**-capped QDs are not stable in aqueous solution due to protonation of the carboxylate groups and subsequent precipitation.

We first started to examine light-driven hydrogen evolution upon irradiation of the three-component system containing red QDs (3.3(±0.1) nm diameter) having **MPA** as capping agent and optimized the conditions by varying the concentration of either the nickel catalyst or the sacrificial agent. Preliminary considerations on the performance of the process can be drawn by looking at the kinetics shown in Figure 3 and 4. Attention has been paid to the estimation of the hydrogen evolution rates, extracted from the slope of the curves in the linear section, and to the maximum quantity of hydrogen produced, represented by the plateau value, as well as to the corresponding values of maximum TOF and TON, respectively, obtained by normalizing maximum rate and amount of H_2 produced by the catalyst concentration.

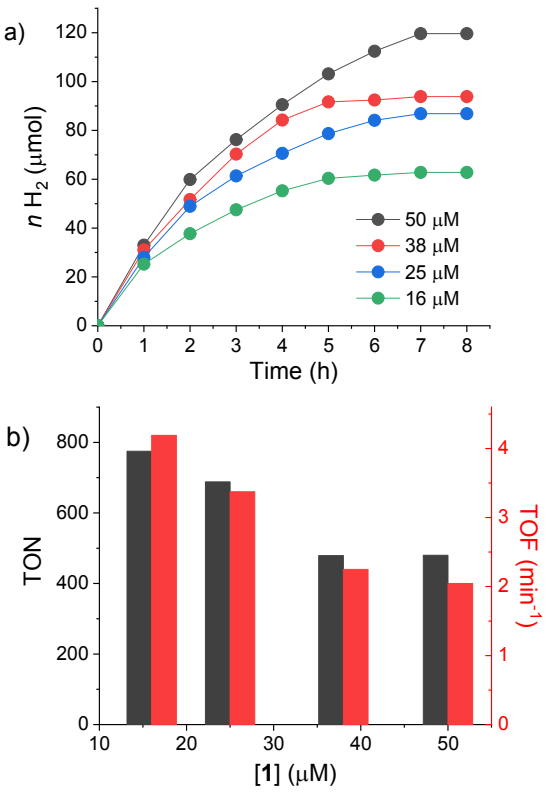

Fig. 3. a) Moles of H_2 produced vs time upon irradiation for **MPA** QDs with d = 3.3 nm by varying the concentration of **1** ([QDs] = 2.6 μM, buffer ascorbate = 1.68 M, pH = 5, Ar-purged solutions) and (b) corresponding maximum TONs and TOFs.

Upon continuous visible-light irradiation of the three-component system, hydrogen production is observed, as detected by GC analysis, for up to 8 h. In the presence of 1.68 M ascorbic acid at pH 5, both the hydrogen evolution rate and maximum amount of hydrogen produced increase with increasing catalyst concentration from 16 μM to 50 μM **1** (Figure 3a). Maximum TONs between 480 and 780 and maximum TOFs between 2.0 and 4.1 min^{-1} can be estimated under these conditions, with the highest values attained at the lowest catalyst concentration tested (Figure 3b). Control experiments conducted in the absence of the nickel complex **1** show that negligible hydrogen is produced (maximum quantity of ~2 μmol after 8 h irradiation), suggesting the key role of the nickel complex in accelerating hydrogen production. On the other hand, by fixing the catalyst concentration at 50 μM and varying the quantity of ascorbate donor in the solution at pH 5, both the rate and the amount of hydrogen produced at plateau are maximized for a 1.68 M concentration of sacrificial agent (Figure 4). We then decided to test **MPA** QDs with different

colours and sizes, namely 1.7, 2.4, 2.8, and 3.1, and QDs with comparable size but different capping agent. Concentrations of 50 μM and 1.68 M of catalyst **1** and sacrificial agent, respectively, have been employed, corresponding to the optimized conditions extracted for **MPA**-capped QDs.

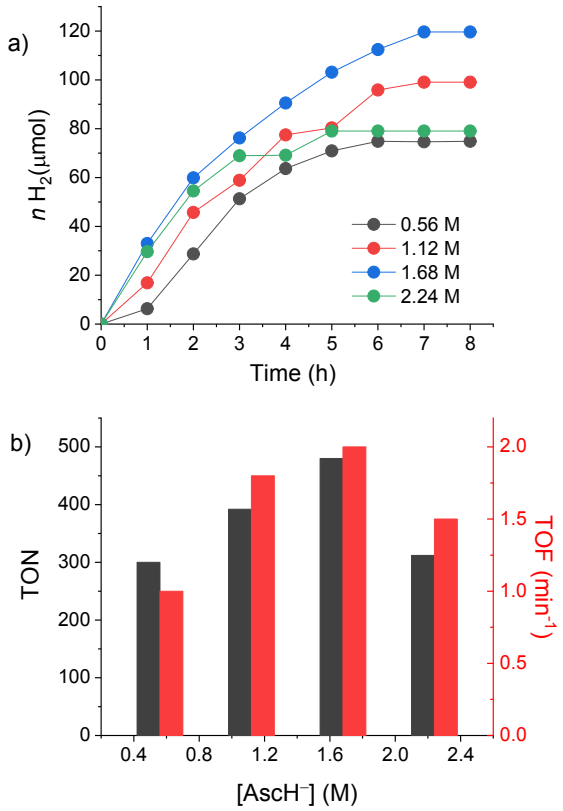

Fig. 4. a) Moles of H_2 produced vs time upon irradiation for **MPA** QDs with d = 3.3 nm by varying the concentration of ascorbate at pH 5 ([QDs] = 2.6 μM, [**1**] = 50 μM, Ar-purged solutions) and (b) corresponding maximum TONs and TOFs.

From the comparison in Figure 5a,b it can be observed that, under full spectrum irradiation, QDs with decreasing size exhibit lower hydrogen evolution rates and total amount of product at plateau. Interestingly, this is true in the case of all stabilizing agents (Figure S15, S16). At first glance, considering that irradiation is performed with a polychromatic source (xenon lamp, 400-700 nm wavelength range), these differences could be related to the different absorption properties of the QDs since larger (i.e., more red-shifted) QDs are expected to absorb a larger fraction of the incoming light source. In order to rule out this hypothesis, we thus normalized the photocatalytic response and in particular the hydrogen evolution rate by a suitable parameter accounting for the fraction of absorbed photons from the Xe light source (see inset in Figure 5c). Although the differences in hydrogen evolution rates (and the derived TOF values, Figure 5c) are somewhat attenuated with this procedure, these results still confirm that the hydrogen evolution performances increase with increasing the size of the QDs. These results contrast with the data reported by Osterloh and co-workers on hydrogen evolution promoted by 2-mercaptoethanol-stabilized CdSe QDs in water at pH 9.2 using Na_2SO_3 as the sacrificial donor.[59,60] Possible reasons can be related to the different nature and energetics of the CdSe QDs as well as to the specific synthetic protocol of the CdSe samples used in that work and the corresponding photophysical properties (actually unknown)[59,60] compared to those of our QDs. Under optimized conditions, a quantum yield of Φ = 0.6% has been estimated for light-driven hydrogen evolution by **MPA**-capped QDs.‡

View Article Online DOI: 10.1039/C5DT01195A

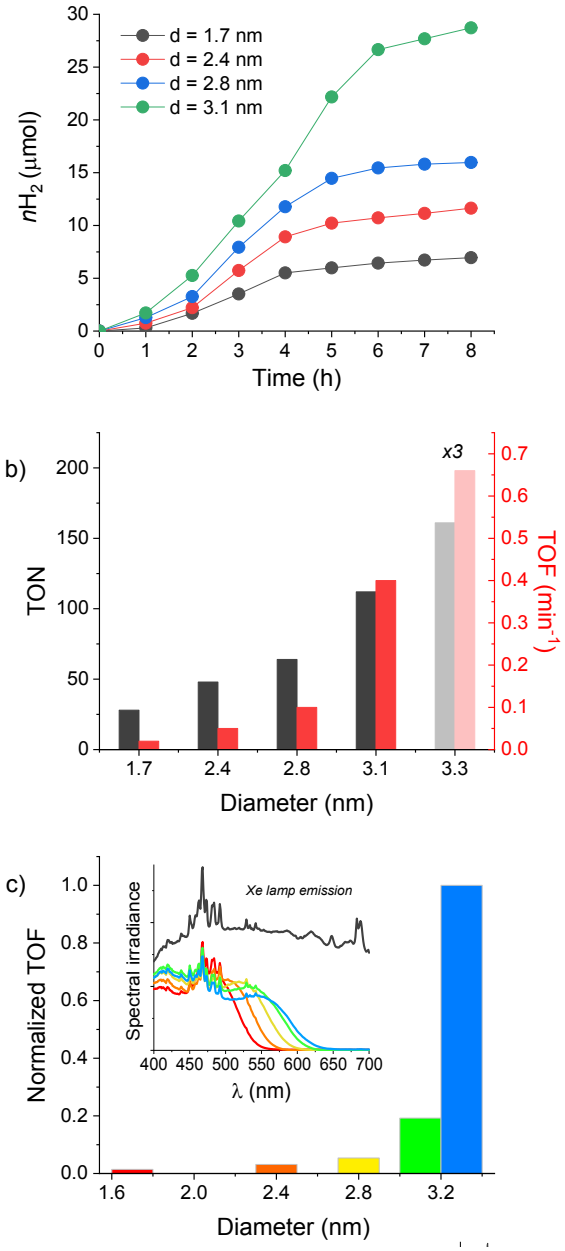

Fig. 5. a) Moles of H_2 produced vs time upon irradiation at pH = 5 for **MPA** QDs with different diameters ([QDs] = 2.6-8.9 μM depending on the size,[50] buffer ascorbate = 1.68 M, [**1**] = 50 μM, Ar-purged solutions); b) corresponding maximum TONs and TOFs values; (c) maximum TOFs normalized with respect to the fraction of photon absorbed for **MPA** QDs with different diameters, (inset) fraction of the Xe lamp emission absorbed by the QDs tested.

Finally, the effect of the capping agent was considered under identical experimental conditions. Green emissive (d = 2.7(±0.1) nm) **MPA**- and **MSA**-capped QDs perform similarly and both

View Article Online DOI: 10.1039/C5DT01185A

better than both **MAA**- capped QDs (Figure S15), whereas in the case of yellow emissive (d = 3.3(±0.1) nm) QDs the **MPA**-capped sample performs significantly better than both **MSA**- and **MAA**-capped QDs analogues (Figure S16). It should be noticed that, in this respect, all the comparisons have been made by normalizing the TOF parameter with respect to the absorbed photons in order to account for the slightly different absorption properties of the QDs with different capping agents. Overall, in all cases, **MAA**- and **MPA**-capped QDs result the less efficient and better performing samples, respectively, towards light-driven hydrogen evolution (Figure S16b).

As to the turnover limiting reactions, theoretically, the maximum amount of hydrogen that can be produced in a three-component system involving ascorbate as the sacrificial agent corresponds to the number of moles of electron donor.[11] From the comparison between the theoretical and the experimental data, the ascorbate consumed in the conditions of maximum hydrogen production is equal to ca 20%. Therefore, the photocatalytic activity is not limited by consumption of the sacrificial agent. The degradation of coordination complexes used as catalysts is known and observed in systems of this type, thus it may be one of the possible reasons for photocatalysis deactivation.[62] At the same time, deactivation of the QD sensitizers can be considered and is supported by visual analysis of the photocatalytic mixture which, once the photocatalysis process ceases, presents a brown precipitate. This can be very reasonably ascribed to the progressive aggregation of the nanoparticles, following the breakdown of the binder layers. This hypothesis has been further confirmed by TEM analysis of the precipitate which shows the presence of large aggregates (Figure S17). The size distribution, obtained by STEM analysis, is rather polydisperse with nanoparticles displaying an average diameter of ca 5 nm (Figure S17), suggesting a sort of re-crystallization process induced by the photocatalysis experiment. Interestingly, the photocatalysis experiment is not apparently affecting the composition of the sample (Table S1), nor the crystal phase of the QDs. Importantly, this material is inactive towards light-driven hydrogen evolution. As a matter of fact, after centrifugation and subsequent redispersion of the post-catalytic material in a fresh solution of **1** and ascorbate at pH 5, negligible amount of hydrogen is produced upon irradiation.

From the data obtained above, two consideration can be made in order to compare the results here reported with those of analogue systems and to rationalize the observed trend in hydrogen evolution performances. (i) Under comparable operating conditions, the **MPA**-capped QDs are better sensitizers than the $Ru(bpy)_3^{2+}$ chromophore in combination with the same nickel catalyst **1** and the ascorbate donor, particularly in terms of moles of hydrogen produced over time and the corresponding TON value.[46] This can be partly explained considering the greater stability of semiconductors with respect to molecular chromophores such as coordination complexes, which are known to display enhanced degradation routes at both the excited state and reduced level.[63-65] (ii) The results reported herein for the samples with **MPA**-capped QDs with 3.3 nm diameter are in line with those previously reported by Llobet and co-workers using red, MPA-capped CdTe QDs in combination with a cobalt macrocyclic complex.[49] (iii) The efficiency and performance of the investigated photocatalytic system depend on the characteristics of the QDs, i.e., their size and the stabilizing agent used. This issue will be discussed in more detail hereafter.

Characterization of the photocatalytic system

In order to clarify the origin of the size-dependent activity as well as the effect of the different capping agents, we first performed a photophysical characterization of the three component system. As reference systems for the following analysis, we took two different samples per capping agents, namely QDs of d = 2.7(±0.1) nm and 3.3(±0.1) nm.

To allow the production of hydrogen as a result of continuous irradiation with QDs as the sensitizers, it is necessary that after excitation the electrons in the conduction band (CB) of the QDs are transferred to the catalyst and the holes in the valence band (VB) are transferred to the sacrificial donor. As previously mentioned, these processes are thermodynamically allowed for all systems. On the other hand, these processes compete with the deactivation associated to the photogenerated electron-hole pair, as a consequence they have to be fast enough to be efficient. Luminescence measurements on QDs in the presence of different quantities of **1** have been performed to verify the feasibility and efficiency of the electron transfer from the CB of the QDs to the nickel complex (Figure S18-S20). In all cases addition of **1** leads to a decrease of the emission intensity which confirms the occurrence of the electron transfer process here considered. The efficiencies are dependent on the catalyst concentration and range between 33-45% for all the samples examined at a concentration of [**1**] = 50 μM. Stern-Volmer analysis (Figure S21) has been then applied to the emission data to gain further mechanistic understanding. From the fitting of experimental data according to the equation $I_0/I = 1 + K_{sv}$ [**1**], K_{sv} have been extracted, which enable to calculate k_Q (Table S2) from the relationship $K_{sv} = k_Q \cdot \tau_0$. The values obtained are in the order of ~10^{11} $M^{-1}s^{-1}$ and are thus incompatible with a dynamic quenching mechanism. On the contrary, they suggest a predominantly static contribution in which quenching by the catalyst occurs within catalyst/QDs adducts formed via pre-association at the ground state level. This association can be promoted either by the presence of carboxylate groups in the catalyst or by electrostatic and/or hydrophobic interactions. The static nature of the quenching process is further supported by time-resolved luminescence measurements which show the same average lifetime for the QDs in the absence and in the presence of complex **1** (Figure S22). Based on these considerations, we can state that the efficiency of the oxidative quenching of the excited state depends only on the equilibrium constant for the formation of the hybrid adducts, namely K_{sv}. Accordingly, quenching by the catalyst is more efficient for QDs with d = 3.3(±0.1) nm. The enhanced surface area in the largest QDs may possibly account for this evidence. Furthermore, the larger driving force for the ET from the CB to the nickel catalyst **1** with decreasing nanocrystal size, as previously inferred from

View Article Online
DOI: 10.1039/D0DT04125A

the data in Table 2, does not represent a relevant factor in the efficiency of the catalyst activation step. Finally, no particular differences are found when different capping agents are considered. This may suggest that the efficiency of the electron transfer from the CB to catalyst **1** is not a determining factor in promoting enhanced hydrogen evolution.

We then evaluated the efficiency of the electron transfer process involving the ascorbate donor and the VB of the QDs. Emission spectra of QDs in the presence of 1.68 M ascorbate at pH 5 have been thus recorded and compared with those in the absence of the donor (Figure S23-S25). From this comparison it can be seen that, in the presence of the sacrificial agent, the emission is red shifted and significantly reduced in intensity. The red shift induced by the ascorbate donor has been already observed on QDs at large donor concentrations[45] and might be related to the presence of interactions between the QDs and the sacrificial agent, given the high concentration of the latter. On the other hand, the observed quenching of the emission in the presence of ascorbate suggests that the photoinduced electron transfer from the donor to the VB takes place efficiently for all the samples analysed. However, given the observed red shift, estimation of the efficiency of the electron transfer process from the emission spectrum cannot be accurately performed. We thus measured the lifetime by TC-SPC in the presence and absence of ascorbate buffer (Figure S26-S31). In all cases a faster decay of the emission is observed, due to the occurrence of the electron transfer from the ascorbate to the VB of the QDs, and from these values quenching efficiencies ranging between 57-95% can be determined (Table S3). These values are generally higher for the **MSA-** and **MAA-**capped QDs than for the **MPA-**capped ones. This apparently contradicts what is shown in the hydrogen production tests under continuous irradiation, in which the best photocatalytic performances have been observed for the **MPA** samples. Probably, the intrinsic characteristics of the QDs rather than the efficiency of the individual electron transfer processes, play an important role in the performances observed in photocatalysis.

In order to rationalize the trend in hydrogen evolution activity experimentally determined, we may recall the photophysical results previously described (Table 1) and match these values with the efficiency measured in photocatalytic tests. As a matter of fact, from a closer inspection of the data, it can be observed that longer lifetimes and higher emission quantum yields are always accompanied by faster photocatalytic production of hydrogen under comparable experimental conditions, with **MPA** QDs of 3.3 nm diameter delivering the highest quantity of hydrogen (120 μmol) after 8 hours irradiation with faster rates when combined with 50 μM **1** and 1.68 M buffer at pH = 5. As previously outlined, small emission quantum yields and lifetimes are related to enhanced non-radiative deactivations ascribable to a larger concentration of surface defects within the QDs. Surface defects determine the presence of intra-band gap electronic states which may act as competitive recombination channels with respect to the forward charge separation and accumulation processes on the catalyst platform, necessary to efficient hydrogen production. According to these considerations, the **MAA-** and **MSA-**capped QDs are expected to possess a greater concentration of surface defects than the **MPA** QDs of identical size. Also, with the same capping agent, QDs with increasingly smaller sizes prepared using the present synthetic approach[48] display larger concentration of surface defects and a corresponding decrease of hydrogen evolution performance in the three-component system examined. Hence, from the experimental data it can be concluded that, in order to obtain sustained hydrogen evolution using QDs and, more generally, semiconductor nanocrystals, large emission quantum yields and long lifetimes are desirable. Accordingly, a thorough control of the synthetic protocol of the target QDs is of imperative importance as is the detailed assessment of the corresponding photophysical properties. To this respect, the choice of the capping agent as well as the suitable choice of the nanocrystal size is of remarkable importance towards profitable applications. Consistent with the results reported herein, it is indeed not surprising that most of the photocatalytic systems for H_2 production reported to date, using CdTe QDs (or, most likely, mixed CdTe/CdS QDs)[48,53,54] as photosensitizers, have been prepared with **MPA** as the capping agent and employing red absorbing nanocrystals.[42,43,45]

Charge carrier dynamics in photoassisted H_2 evolution

As previously outlined, excitonic charge carriers (i.e., electrons and holes at the band edges) play a determining role in light-driven hydrogen evolution within the three-component system using QDs with **1** and ascorbate as the catalyst and the donor, respectively. However, the previous investigation does not give information as to the potential role of trapped charge carriers within the photocatalytic process. Indeed, while the emission measurements provide information as regarding the reactivity of photogenerated electrons and holes in the energy levels characteristic of the exciton (i.e., at the CB and VB band edges, respectively), they do not provide indications as far as the reactivity of charge carriers in trap states is concerned.

In order to characterized the charge carrier dynamics at the basis of photoinduced hydrogen evolution, we chose the best performing system (namely **MPA**-capped QDs of 3.3 nm diameter) and performed transient absorption spectroscopy measurements by nanosecond laser flash photolysis under the experimental conditions used in the hydrogen evolution tests (Figure 6).

In the absence of both the donor and the nickel catalyst **1**, the transient spectrum sampled at 180 μs after the laser pulse is characterized by a bleaching at wavelengths between 540 and 640 nm and an absorption at wavelengths greater than 640 nm (Figure 6a). The negative signal corresponds to the bleaching of the excitonic transition due to the depopulation of the ground state, while the positive signal is attributable to the absorption of charge carriers, in particular of trapped holes.[45,66] This spectrum decays towards the baseline (isosbestic point at 640 nm and $\Delta OD = 0$) consistent with the repopulation of the ground state. The lifetime measured at 580 nm ($\tau \sim 7$ ms, Figure S32) is considerably greater than the one measured by emission. This allows us to infer that the transient spectrum here detected is

View Article Online
DOI: 10.1039/D0DT04195A

ascribable to the formation of intra-bandgap states, likely involving both photogenerated electrons and holes, which decay to the ground state in the ms timescale (Figure 6a).

In the presence of the ascorbate donor, two effects can be observed: i) the amount of transient sampled at 180 µs (Figure 6b) is considerably smaller and corresponds to ca a half of the same signal in the QDs sample alone (Figure 6a), ii) the transient spectrum at 180 µs, previously associated to charge carriers in the intra-bandgap states, decays more rapidly (τ ~ 0.4 ms, Figure S33) forming an absorption with two maxima at 580 and 620 nm which remains stable in a longer timescale (>10 ms), and can be associated to photogenerated electrons, in analogy to the corresponding fingerprint in other semiconducting materials.[67,68]

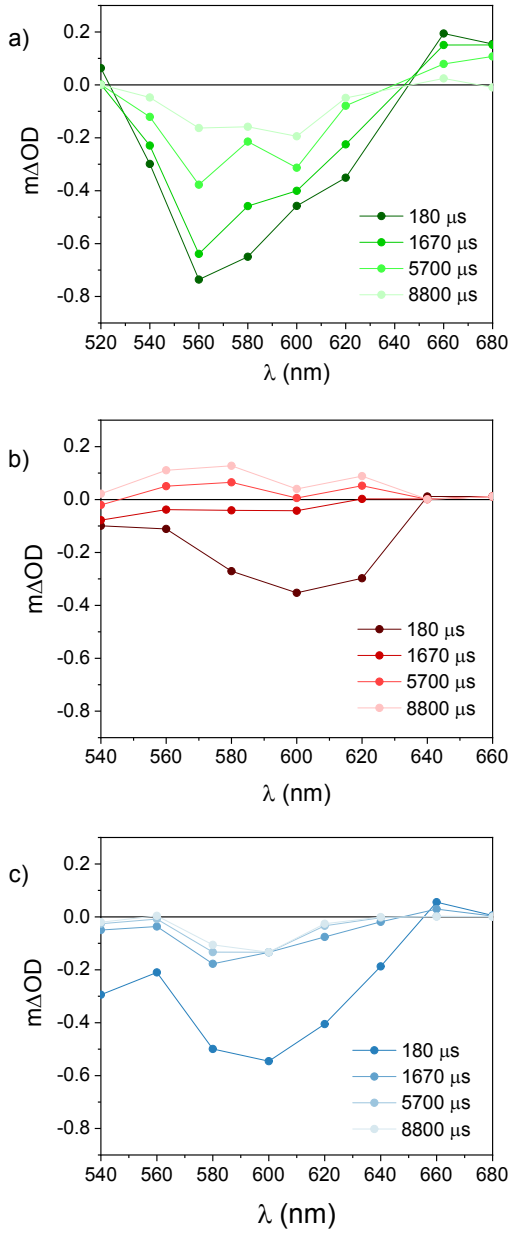

Fig. 6. Transient absorption spectra of a) **MPA** QDs (2.6 µM), b) **MPA** QDs (2.6 µM) in the presence of ascorbate buffer (1.68 M), and (c) **MPA** QDs (2.6 µM) with both the ascorbate buffer and the nickel catalyst **1** (50 µM), obtained by laser flash photolysis (excitation at 532 nm, Ar-purged solutions).

These evidences confirm that: i) an aliquot of trap states (ca a half) is not populated due to the direct (fast) reaction of the holes at the VB edge with the ascorbate donor, according to the emission measurements reported above, ii) a fraction of surface trapped holes reacts irreversibly with the ascorbate donor. This reaction sequence leaves long-lived electrons in the QDs as evidenced by the stable, broad absorption in the visible spectrum between 540-640 nm.

In the presence of both the ascorbate donor and the catalyst **1** (Figure 6c), the transient spectrum associated to trapped charge carriers decays rapidly (τ ~ 0.5 ms Figure S34) due to the reaction of the holes with the donor as observed before (Figure 6b). However, the lack of any long-lived positive signals suggests that photogenerated electrons are efficiently and quickly transferred to the nickel catalyst **1**.

A resume of the photophysical data is reported in Figure 7, which combines the previous considerations from steady-state and time-resolved emission with the transient absorption data.

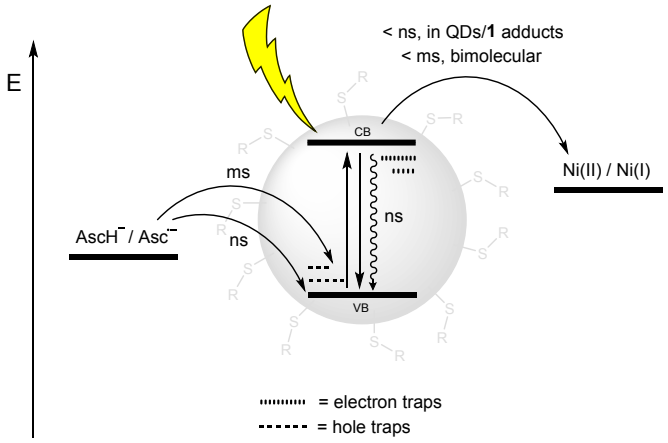

Fig. 7. Summary of the primary photoinduced processes with related timescale.

Accordingly, we can summarize that upon photoexcitation: i) holes at the VB band edge react in the ns timescale with remarkable efficiency with the ascorbate donor, ii) a fraction of trapped holes reacts with the same sacrificial agent in the ms time-scale, iii) photogenerated electrons are efficiently transferred to the nickel catalyst **1**. As to the latter point, formation of QDs/catalyst adducts are expected to foster the forward electron transfer cascade at the basis of hydrogen evolution. Rates in the sub-ns timescale are indeed expected according to time-resolved emission measurements. Nevertheless, the intrinsic high efficiency in the hole-scavenging process and the failure to observe any long-lived electrons in the three-component system (Figure 5c) very likely suggest that bimolecular electron transfer processes from the QDs to catalyst **1** might be efficient as well.

The experimental observation of trapped charge carriers by laser flash photolysis points towards an active role of trap states in the photocatalytic process. Similarly, it can be also envisaged that trap states (in particular deep trap states) may be actively involved in detrimental charge recombination pathways, thus affecting light-driven hydrogen evolution activity, as previously inferred.

View Article Online
DOI: 10.1039/D0DT04195A

Experimental Section

Materials and methods.

All reagents were purchased from sigma Aldrich and used as received. Milli-Q water was obtained using a Millipore apparatus, equipped with 0.22 μm filters. The nickel complex **1**, available from a previous study,[46] was used. Absorption spectra were registered on a Cary 300 UV-Vis (Agilent Technologies) spectrophotometer. Emission spectra were taken on an Edinburgh FLS 920 spectrofluorometer. Emission lifetimes on the same samples were acquired with a Picoquant Picoharp 300 time correlated single photon counting at a 4 ps resolution by using a 480 nm pulsed LED source. Fitting of the decay histogram was accomplished by a dedicated Fluofit program. Nanosecond transient measurements were performed with a custom laser spectrometer comprised of a Continuum Surelite II Nd:YAG laser (FWHM 6 – 8 ns) with frequency doubled (532 nm) option, an Applied Photophysics xenon light source including a mod. 720 150W lamp housing, a mod. 620 power-controlled lamp supply and a mod. 03 −102 arc lamp pulser. Laser excitation was provided at 90° with respect to the white light probe beam and was attenuated to an average power of 5 mJ/pulse using a series of neutral density filters (Edmund Optics). Light transmitted by the sample was focused onto the entrance slit of a 300 mm focal length Acton SpectraPro 2300i triple grating, flat field, double exit monochromator equipped with a photomultiplier detector (Hamamatsu R3896). Signals from the photomultiplier (kinetic traces) were processed by means of a TeledyneLeCroy 604Zi (400 MHz, 20 GS/s) digital oscilloscope.

Cyclic voltammetry (CV) measurements were carried out on a PGSTAT 302N potentiostat (Autolab) in a three-electrode cell, using a saturated calomel electrode (Amel) as reference electrode, a glassy carbon as working electrode and a Pt wire as counter electrode. CV measurements at a scan rate of 20 mV/s were conducted directly on the aqueous solutions obtained from the synthetic process upon addition of 0.1 M $LiClO_4$ as the supporting electrolyte.

High Resolution Transmission Electron Microscope (HR-TEM) characterization was carried out with a FEI Tecnai F20 field emission instrument, operated at 200 keV. Scanning transmission electron microscopy (STEM) mode, coupled with high angle annular dark field (HAADF) detector and Energy Dispersive X-Ray spectroscopy (EDS) were employed to perform size distribution analysis as well as to detect sample composition and elemental distribution. TEM grids were prepared by drop casting the QDs solution on a continuous Formvar film coated Cu grid. No evidence of deposition-induced structural change or aggregation was observed.

The light-driven hydrogen evolution experiments were carried out upon continuous visible-light irradiation of a reactor containing the solution (a 10 mm pathlength pyrex glass cuvette with head space obtained from a round-bottom flask). Solutions were purged using argon gas for 15 minutes prior to irradiation. A 175 W Xenon light was used as the light source, a cut-off filter at λ = 400 nm and a hot mirror were employed providing a suitable irradiation between 400 and 700 nm. The gas phase of the reaction vessel was analysed on an Agilent Technologies 490 microGC equipped with a 5 Å molecular sieve column (10 m), a thermal conductivity detector, and using argon as carrier gas. Additional details of the setup and procedures used for the hydrogen evolution experiments can be found in previous reports.[23,64,65]

Synthesis of QDs.

QDs capped with **MAA** (mercaptoacetic acid), **MPA** (mercaptopropionic acid) and **MSA** (mercaptosuccinic acid) were synthetized according to a literature procedure.[48] The molar ratio of Cd^{2+}/stabilizing agent/TeO_3^{2-} was 1 : 1 : 0.2. Briefly, 0.4 mmol of $CdCl_2$ was dissolved into 100 mL deionized water. Then 0.4 mmol of stabilizing agent (**MAA**, **MPA** or **MSA**) were added and the pH was adjusted with 1 M NaOH solution to the value of 10.5. After stirring for 5 min, 0.08 mmol of K_2TeO_3, which dissolved in 100 mL deionized water, were added into the above solution. Then, 160 mg of $NaBH_4$ were added into the precursor solution. After the reactions proceeded for other 5 minutes, the flask was attached to a condenser and refluxed at 100 °C under open-air conditions. Through controlling the reaction time, QDs with desired optical properties were obtained.

Conclusions

In this work CdTe/CdS QDs with different sizes and capping agents (i.e., **MPA**, **MAA** and **MSA**) have been synthesized. The samples have been characterized by conventional techniques such as UV-Visible absorption and emission spectroscopy and cyclic voltammetry. Structural characterization has been accomplished by means of HR-TEM/EDS which suggests the formation of mixed CdTe/CdS QDs. The synthesized QDs samples have been tested for photoinduced hydrogen evolution in combination with the nickel DuBois catalyst **1** and ascorbate as the sacrificial electron donor. The results show that all the prepared systems are active towards hydrogen production under visible light irradiation, outperforming the standard $Ru(bpy)_3^{2+}$ chromophore. QDs with **MPA** as stabilizing agents and diameter of d = 3.3 nm have been identified as the best sample with maximum quantities of hydrogen produced upon irradiation equal to 120 μmol using 50 μM **1** and 1.68 M ascorbate at pH 5. More importantly, the efficiency of the photocatalytic system based on QDs improves as the size of the nanoparticles increases and using **MPA** as stabilizing agent rather than **MAA** or **MSA**. The trend in hydrogen evolution photoactivity parallels the trend in luminescence quantum yield and lifetime and is consistent with a lower surface defectiveness of the QDs with larger dimensions and **MPA** capping agent. Overall, the present work clearly highlights the role of semiconducting nanocrystals as suitable sensitizers for energy conversion schemes and evidences how a careful adjustment and regulation of the surface properties is of pivotal importance in order to optimize the photocatalytic performance in view of potential applications.

Conflicts of interest

There are no conflicts to declare.

Acknowledgements

M. N. gratefully acknowledges Dr. Diego Guzmán (Universidad Tecnológica Metropolitana, Santiago, Chile) for fruitful discussions. Financial supports from the University of Ferrara (FAR2019) are gratefully acknowledged.

Notes and references

¶ The potentials of the CB for red-absorbing QDs, here calculated, are less negative than those reported by Wu and co-workers for CdTe QDs of similar size.[35,57] This difference stems from the more positive VB potential considered (+0.09 V vs. NHE) and obtained by pulse radiolysis.[58] We would like to point out that, assuming this latter value for the VB potential in our system, oxidation of the ascorbate donor at pH 5 (+0.4 V vs. NHE) would not be thermodynamically allowed.

‡ The quantum yield of hydrogen evolution (Φ) has been estimated from the ratio between the initial rate of hydrogen production ($5.0 \cdot 10^{15}$ H_2 molecules/s corresponding to a rate of 30 μmol/h) and the absorbed photon flux ($8.3 \cdot 10^{17}$ photons/s, Figure S35) estimated by integration considering the spectral irradiance of the Xe lamp used in our setup, the LHE of the irradiated solution and the irradiated surface area (5 cm^2). Considering that the maximum value of Φ in photoinduced hydrogen formation with the three-component system here used is 50%,[11] this value translates into an overall quantum efficiency (QE)[61] of 1.2%.

1 N. S. Lewis and D. G. Nocera, *Proc. Natl. Acad. Sci. U.S.A.,* 2006, **103**, 15729.
2 M. Natali and F. Scandola, Supramolecular artificial photosynthesis, *Applied Photochemistry: When Light Meets Molecules, Lecture Notes in Chemistry*, 2016, ed. G. Bergamini, S. Silvi, Springer.
3 T. R. Cook, D. K. Dogutan, S. Y. Reece, Y. Surendranath, T. S. Teets and D. G. Nocera, *Chem. Rev.,* 2010, **110**, 6474.
4 J. A. Turner, *Science*, 1999, **285**, 687.
5 M. G. Walter, E . L. Warren, J. R. McKone, S. W. Boettcher, Q. Mi, E. A. Santori and N. S. Lewis, *Chem. Rev.*, 2010, **110**, 6446.
6 J. Yang, D. Wang, H. Han and C. Li, *Acc. Chem. Res.*, 2013, **46**, 1900.
7 V. Artero and J. M. Saveant, *Energy Environ. Sci.*, 2014, **7**, 3808.
8 M. Yu, F. Li and L. Sun, *Energy Environ. Sci.*, 2015, **8**, 760.
9 B. D. Sherman, M. V. Sheridan, K.-R. Wee, S. L. Marquard, D. Wang, L. Alibabaei, D. Ashford and T. J. Meyer, *J. Am. Chem. Soc.*, 2016, **138**, 16745.
10 B. Shan, A. K. Das, S. Marquard, B. H. Farnum, D. Wang, R. M. Bullock and T. J. Meyer, *Energy Environ. Sci.*, 2016, **9**, 3693.
11 Y. Pellegrin and F. Odobel, *C.R. Chim.*, 2017, **20**, 283.
12 K. Ladomenou, M. Natali, E. Iengo, G. Charalampidis, F. Scandola and A. G. Coutsolelos, *Coord. Chem. Rev.*, 2015, **304-305**, 38.
13 E. S. Andreiadis, M. Chavarot-Kerlidou, M. Fontecave and V. Artero, *Photochemistry and Photobiology*, 2011, **87**, 946.
14 W. K. C. Lo, C. E. Castillo, R. Gueret, J. Fortage, M. Rebarz, M. Sliwa, F. Thomas, C. J. McAdam, G. B. Jameson, D. A. McMorran, J. D. Crowley, M. N. Collomb and A. G. Blackman, *Inorg. Chem.*, 2016, **55**, 4564.
15 a) E. Deponti, A. Luisa, M. Natali, E. Iengo and F. Scandola, *Dalton Trans.*, 2014, **43**, 16345. b) M. Natali, E. Badetti, E. Deponti, M. Gamberoni, F. A. Scaramuzzo, A. Sartorel and C. Zonta, *Dalton Trans.*, 2016, **45**, 14764.
16 J. I. Goldsmith, W. R. Hudson, M. S. Lowry, T. H. Anderson and S. Bernhard, *J. Am. Chem. Soc.,* 2005, **127**, 7502.
17 B. Probst, M. Guttentag, A. Rodenberg, P. Hamm and R. Alberto, *Inorg. Chem.*, 2011, **50**, 3404.
18 B. Probst, A. Rodenberg, M. Guttentag, P. Hamm and R. Alberto, *Inorg. Chem.*, 2010, **49**, 6453.
19 B. Probst, C. Kolano, P. Hamm and R. Alberto, *Inorg. Chem.*, 2009, **48**, 1836.
20 P. Du, J. Schneider, P. Jarosz and R. Eisenberg, *J. Am. Chem. Soc.*, 2006, **128**, 7726.
21 T. T. Li, Y. Chen and W. F. Fu, *Catal. Commun.,* 2014, **45**, 91.
22 P. Du, J. Schneider, P. Jarosz, J. Zhang, W. W. Brennessel, R. Eisenberg, *J. Phys. Chem. B*, 2007, **111**, 6887.
23 M. Natali, R. Argazzi, C. Chiorboli, E. Iengo and F. Scandola, *Chem. Eur. J.*, 2013, **19**, 9261.
24 T. Lazarides, M. Delor, I. V. Sazanovich, T. M. McCormick, I. Georgakaki, G. Charalambidis, J. A. Weinstein and A. G. Coutsolelos, *Chem. Comm*., 2014, **50**, 521.
25 A. Panagiotopoulos, K. Ladomenou, D. Y. Sun, V. Artero and A. G. Coutsolelos, *Dalton Trans*, 2016, **45**, 6732.
26 G. Landrou, A. A. Panagiotopoulos, K. Ladomenou, A. G. Coutsolelos, *J. Porph. Phthal.*, 2016, **20**, 534.
27 N. Queyriaux, E. Giannoudis, C. D. Windle, S. Roy, J. Pecaut, A. G. Coutsolelos, V. Artero and M. Chavarot-Kerlidou, *Sustainable Energy Fuels*, 2018, **2**, 553.
28 E. Nikoloudakis, K. Karikis, J. J. Han, C. Kokotidou, A. Charisiadis, F. Folias, A. M. Douvas, A. Mitraki, G. Charalambidis, X. H. Yan and A. G. Coutsolelos, *Nanoscale* 2019, **11**, 3557.
29 S. Salzl, M. Ertl and G. Knor, *Phys. Chem. Chem. Phys.* 2017, **19**, 8141.
30 E. Giannoudis, E. Benazzi, J. Karlsson, C. Graeme, S. Panagiotakis, G. Landrou, P. Angaridis, V. Nikolaou, C. Matthaiaki, G. Charalambidis, E. A. Gibson and A. G. Coutsolelos, *Inorg. Chem.* 2020, **59**, 1611.
31 a) G. D. Scholes, *Adv. Funct. Mater.*, 2008, **18**, 1157. b) D. A. Wheeler and J. Z. Zhang, *Adv. Mater.*, 2013, **25**, 2878.
32 J. X. Jian, Q. Liu, Z. J. Li, F. Wang, X. B. Li, C. B. Li, B. Liu, Q. Y. Meng, B. Chen, K. Feng, C. H. Tung and L. Z. Wu, *Nat. Commun.,* 2013, **4**, 2695.
33 F. Wen, J. Yang, X. Zong, B. Ma, D. Wang and C. Li, *J. Catal.,* 2011, **281**, 318.
34 Z. Han, F. Qiu, R. Eisenberg, P. L. Holland and T. D. Krauss, *Science*, 2012, **338**, 1321.
35 C. B. Li, Z. J. Li, S. Yu, G. X. Wang, F. Wang, Q. Y. Meng, B. Chen, K. Feng, C. H. Tung and L. Z. Wu, *Energy Environ. Sci.*, 2013, **6**, 2597.
36 C. Baslak, E. Aslan, I. H. Patir, M. Kus and M. Ersoz, *Int. J. Hydr. Energy*, 2016, **41**, 20523.
37 Z. Han and R. Eisenberg, *Acc. Chem. Res*., 2014, **47**, 2537.
38 F. Wen, X. Wang, L. Huang, G. Ma, J. Yang and C. Li, *ChemSusChem*, 2012, **5**, 84.
39 X. W. Song, H. M. Wen, C. B. Ma, M. Q. Hu, H. H. Cui and C. N. Chen, *Appl. Organomet. Chem.,* 2014, **28**, 267.
40 J. Huang, K. L. Mulfort, P. Du and L. Chen, *J. Am. Chem. Soc.,* 2012, **134**, 16472.
41 M. Sandroni, R. Gueret, K. D. Wegner, P. Reiss, J. Fortage, D. Aldakov and M.-N. Collomb, *Energy Environ. Sci*., 2018, **11**, 1752.
42 a) K. A. Brown, S. Dayal, X. Ai, G. Rumbles and P. W. King, *J. Am. Chem. Soc.*, 2010, **132**, 9672. b) K. A. Brown, M. B. Wilker, M. Boehm, G. Dukovic and P. W. King, *J. Am. Chem. Soc.*, 2012, **134**, 5627.
43 B. L. Greene, C. A. Joseph, M. J. Maroney and R. B. Dyer, *J. Am. Chem. Soc.*, 2012, **134**, 11108.

View Article Online
DOI: 10.1039/D0DT01195A

44 K. Han, M. Wang, S. Zhang, S. Wu, Y. Yanga and L. Sun, *Chem. Commun.,* 2015, **51**, 7008.
45 C. Gimbert-Suriñach, J. Albero, T. Stoll, J. Fortage, M.-N. Collomb, A. Deronzier, E. Palomares and A. Llobet, *J. Am. Chem. Soc.* 2014, **136**, 7655.
46 G. Bergamini and M. Natali, *Dalton Trans*., 2019, **48**, 14653.
47 U. J. Kilgore, J. A. S. Roberts, D. H. Pool, A. M. Appel, M. P. Stewart, M. R. DuBois, W. J. Dougherty, W. S. Kassel, R. M. Bullock and D. L. DuBois, *J. Am. Chem. Soc.*, 2011, **133**, 5861.
48 S. Wu, J. Dou, J. Zhang and S. Zhang, *J. Mater. Chem*., 2012, **22**, 14573.
49 C. Mongin, S. Garakyaraghi, N. Razgoniaeva, M. Zamkov and F. N. Castellano, *Science*, 2016, **351**, 369.
50 W. Yu, L. Qu, W. Guo and X. Peng, *Chem. Mater.*, 2003, **15**, 2854
51 K. Nakamaru, *Bull. Chem. Soc. Japan,* 1982, **55**, 1639.
52 A. J. Houtepen, I. Infante, W. Van der Stam, I. du Fossé, H. A. C. Bergstein, G. Grimaldi, R. W. Crisp, J. O. V. Monchen and N. Kirkwood, *J. Am. Chem. Soc*. 2018, **140**, 15712.
53 H. Qian, C. Dong, J. Weng and J. Ren, *Small*, 2006, **2**, 747.
54 E. Ying, D. Li, S. Guo, S. Dong and J. Wang, *PlosONE*, 2008, **3**, e2222.
55 M. Natali, *ACS Catal*. 2017, **7**, 1330.
56 B. H. J. Bielski, A. O. Allen and H. A. Schwarz, *J. Am. Chem. Soc.* 1981, **103**, 3516.
57 a) F. Wang, W. G. Wang, X. J. Wang, H. Y. Wang, C. H. Tung and L. Z. Wu, *Angew. Chem., Int. Ed.*, 2011, **50**, 3193. b) Z. J. Li, X. B. Fan, X. B. Li, J. X. Li, C. Ye, J. J. Wang, S. Yu, C. B. Li, Y. J. Gao, Q. Y. Meng, C. H. Tung and L. Z. Wu, *J. Am. Chem. Soc.*, 2014, **136**, 8261.
58 T. Rajh, O. I. Micic and A. J. Nozik, *J. Phys. Chem.*, 1993, **97**, 11999.
59 M. A. Holmes, T. K. Townsend and F. E. Osterloh, *Chem. Commun*., 2012, **48**, 371.
60 J. Zhao, M. A. Holmes and F. E. Osterloh, *ACS Nano* 2013, **7**, 4316.
61 M. Natali, F. Nastasi, F. Puntoriero and A. Sartorel, *Eur. J. Inorg. Chem.*, 2019, **2019**, 2027.
62 W. T. Eckenhoff, W. R. McNamara, P. Du and R. Eisenberg, *Biochim. Biophys. Acta*, 2013, **1827**, 958.
63 R. S. Khnayzer, V. S. Thoi, M. Nippe, A. E. King, J. W. Jurss, K. A. El Roz, J. R. Long, C. J. Chang and F. N. Castellano, *Energy Environ. Sci.*, 2014, **7**, 1477.
64 M. Natali, A. Luisa, E. Iengo and F. Scandola, *Chem. Commun.*, 2014, **50**, 1842.
65 E. Deponti and M. Natali, *Dalton Trans*., 2016, **45**, 9136.
66 M. Abdellah, K. J. Karki, N. Lenngren, K. Zheng, T. Pascher, A. Yartsev and T. Pullerits, *J. Phys. Chem. C*, 2014, **118**, 21682.
67 A. Kafizas, X. Wang, S. R. Pendlebury, P. Barnes, M. Ling, C. Sotelo-Vazquez, R. Quesada-Cabrera, C. Li, I. P. Parkin and J. R. Durrant, *J. Phys. Chem. A*, 2016, **120**, 715.
68 R. Godin, Y. Wang, M. A. Zwijneenburg, J. Tang and J. R. Durrant, *J. Am. Chem. Soc.*, 2017, **139**, 5216.